The Ellsworth Subglacial Highlands: inception and retreat of the West Antarctic Ice Sheet

Neil Ross[1], Tom A. Jordan[2], Robert G. Bingham[3], Hugh F.J. Corr[2], Fausto Ferraccioli[2], Anne Le Brocq[4], David M. Rippin[5], Andrew P. Wright[4], and Martin J. Siegert[6]

1. School of Geography, Politics and Sociology, Newcastle University, Newcastle upon Tyne, NE1 7RU, UK
2. British Antarctic Survey, Cambridge CB3 0ET, UK
3. School of Geosciences, University of Aberdeen, Aberdeen AB24 3UF, UK
4. School of Geography, University of Exeter, Exeter EX4 4RJ, UK
5. Environment Department, University of York, York YO10 5DD, UK
6. Bristol Glaciology Centre, School of Geographical Sciences, University of Bristol, Bristol BS8 1SS

ABSTRACT

Antarctic subglacial highlands are where the Antarctic ice sheets first developed and the 'pinning points' where retreat phases of the marine-based sectors of the ice sheet are impeded. Due to low ice velocities and limited present-day change in the ice sheet interior, West Antarctic subglacial highlands have been overlooked for detailed study. These regions have considerable potential, however, for establishing from where the West Antarctic Ice Sheet (WAIS) originated and grew, and its likely response to warming climates. Here, we characterize the subglacial morphology of the Ellsworth Subglacial Highlands (ESH), West Antarctica, from ground-based and aerogeophysical radio-echo sounding (RES) surveys and the MODIS Mosaic of Antarctica. We document well-preserved classic landforms associated with restricted, dynamic, marine-proximal alpine glaciation, with hanging tributary valleys feeding a significant overdeepened trough (the Ellsworth Trough) cut by valley (tidewater) glaciers. Fjord-mouth threshold bars down-ice of two overdeepenings define both the northwest and southeast termini of paleo outlet-glaciers which cut and occupied the Ellsworth Trough. Satellite imagery

reveals numerous other glaciated valleys, terminating at the edge of deep former marine basins (e.g. Bentley Subglacial Trench), throughout ESH. These geomorphic data can be used to reconstruct the glaciology of the ice masses that formed the proto-WAIS. The landscape predates the present ice sheet, and was formed by a small dynamic ice-field(s), similar to those of the present-day Antarctic Peninsula, at times when the marine sections of the WAIS were absent. ESH represents a major seeding centre of the paleo-WAIS, and its margins represent the pinning point at which future retreat of the marine-based WAIS would be arrested.

1 INTRODUCTION

The West Antarctic Ice Sheet (WAIS) rests largely on a bed several hundred meters below sea level. As a marine-based ice sheet, it may be inherently unstable due to its sensitivity to ocean temperatures and upstream deepening of its bed in a number of key areas [Weertman, 1974; Bamber et al., 2009; Joughin and Alley, 2011]. However, despite it being critical to our evaluation of WAIS inception, stability, and the likelihood of future sea-level change from ice-sheet loss [Bentley, 2010], the glacial history of West Antarctica is not well constrained.

The recognition that the subglacial highlands of East Antarctica acted as critical nucleation sites for the East Antarctic Ice Sheet has driven much recent research [e.g. Bo et al., 2009; Bell et al., 2011; Ferraccioli et al., 2011]. In comparison, however, the subglacial upland areas of the WAIS have been little investigated. Two dominant upland regions, which may be instrumental in the growth and decay of the ice sheet, exist beneath the WAIS: the Ellsworth Subglacial Highlands (ESH) and the coastal mountain ranges of Marie Byrd Land, centered around the Executive Committee Range (Figure 1a). Bentley et al. [1960] hypothesized that these uplands were the main seeding grounds of WAIS growth, while Bamber et al. [2009] hypothesized them as pinning points of a retreating ice sheet. Testing these hypotheses requires evidence of former ice dynamics. Several investigations in East Antarctica have demonstrated the utility of radio-echo sounding (RES) in mapping ancient glacial geomorphic features from which ice sheet reconstructions can be based [Bo et al., 2009; Young et al., 2011]. Here, we present geophysical data on the morphology of ESH, gained during three seasons of ground-based and airborne RES measurements around Ellsworth Subglacial Lake (ESL) [Woodward et al., 2010] and over the Institute and Möller ice streams (hereafter IIS and MIS; see Figure 1) [Ross et al., 2012]. These surveys have revealed a deep (>2000 m bsl), broad (up to 25 km across) and >300 km long subglacial trough, named 'Ellsworth Trough' (ET), which dissects ESH northwest to southeast (Figure 2). Aligned roughly parallel to linear topographic trends in the Ellsworth Mountains, and bounded on both sides by rugged mountainous subglacial topography, ET is one of a series of northwest to southeast trending subglacial valleys extending from the core of ESH into the Bentley Subglacial Trench (Figure 1), a number of which contain subglacial lakes [Vaughan et al., 2006, 2007]. ET lies roughly orthogonal to the Amundsen-Weddell ice divide [Ross et al., 2011], currently contains ESL [Woodward et al., 2010; Siegert et al., 2012] and hosts an enhanced flow tributary of IIS [Joughin et al., 2006; Rignot et al., 2011] which connects to the deep marine basin that underlies the coastal parts of the IIS and MIS [Ross et al., 2012].

In this paper, we first describe and interpret (i) high-resolution ground-based radar data acquired over the northwestern parts of ET; and (ii) airborne radar data acquired over the southeastern parts of ET. We then combine the bed topographic data with ice-surface remote sensing data to place our interpretation of these data into the broader context of ESH and West Antarctica.

2 METHODS

2.1 Radio-echo sounding, northwestern Ellsworth Trough

Ground-based RES data were acquired over and around ET during the 2007/08 and 2008/09 Antarctic field seasons (Figure 1b and Siegert et al., 2012). Data were acquired with the low frequency (~2 MHz) DELORES (DEep-LOok Radio Echo Sounder) radar (further details of the system are provided in King [2009]). Acquisition was undertaken using half-dipole lengths of 40 m with the system towed behind a snowmobile travelling at ~12 km hr^{-1}. Measurements were stacked 1000 times, giving along-track measurements (traces) every 2-5 m. Roving GPS data, to locate the xyz positions of individual radar traces, were acquired using a GPS antenna secured on the radar receiver sledge. Differential GPS processing used daily precise point positioning (PPP)-processed positions of a GPS receiver, located over the center of ESL, as the fixed reference station. Roving data were corrected for the ~90 m offset between the GPS receiver and the midpoint between the radar transmitter and receiver. Radar data processing, undertaken using REFLEXW processing software, involved: (i) bandpass frequency filtering; (ii) gain correction; and (iii) migration. The peak of the first 'bed' return of each trace was picked and ice thickness was calculated from the two-way-travel time of the bed pick using a velocity of 0.168 m ns^{-1}. No firn correction was applied. Ice thickness was subtracted from the GPS-derived ice surface elevation of each trace to establish bed elevations relative to the WGS84 ellipsoid. DELORES-derived bed elevations were combined with contours from a seismic reflection-derived grid of the floor of ESL [Woodward et al., 2010] and gridded, using the ARCGIS “Topo to Raster” interpolation function, to produce a combined digital elevation model of the sub-ice/sub-lake topography.

2.2 Radio-echo sounding, southeastern Ellsworth Trough

25,000 line km of aerogeophysical survey data were acquired over IIS and MIS during the 2010/11 Antarctic field season (Figure 1b, and Ross et al., 2012). Data were acquired using the British Antarctic Survey (BAS) airborne radar system installed on a ski-equipped Twin Otter aircraft. Full details of data acquisition and processing have been reported previously [e.g. Corr et al., 2007; Ross et al., 2012; Karlsson et al., 2012], but a brief summary is provided here. The ice-sounding radar is a coherent system with a frequency of 150 MHz. Aircraft position and elevation were obtained from onboard differential GPS, corrected using GPS base stations from two remote field camps. The ice sheet surface elevation was established from radar or laser altimeter terrain-clearance measurements. Processing and the semi-automated picking of the radar data were undertaken using PROMAX processing software, with Doppler processing used to migrate radar-scattering hyperbolae in the along-track direction. Ice thickness, at an along-track interval of ~10 m, was calculated from the two-way travel-time of the bed pick using a velocity of 0.168 m ns^{-1} and a firn layer correction of 10 m. Ice thickness was subtracted from the ice surface elevation of each trace to establish bed elevations relative to the WGS84 ellipsoid. Bed elevations were then gridded, using the ArcGIS Natural Neighbor interpolation algorithm, to produce a digital elevation model of the subglacial topography.

2.3 Satellite imagery

The Moderate Resolution Imaging Spectroradiometer (MODIS) Mosaic of Antarctica (MOA) [Scambos et al., 2007] is a digital image mosaic of the surface morphology of the Antarctic ice sheet, derived from red light and infrared imagery of the Antarctic Continent. This mosaic has considerable potential for shedding light on ice sheet flow and sub-ice landforms and structures. We investigated the MODIS MOA imagery (Figure 2a) to assess its ability to reflect underlying subglacial topography. Subglacial topography influences ice surface elevation, and hence ice sheet surface imagery, due to the viscous response of ice as it flows over subglacial relief. Increasing ice thickness acts to damp the response to subglacial topography, so regions of thin ice within subglacial highlands are associated with more rugged surface topography and variable surface imagery than areas of thicker ice. Earlier studies have demonstrated the effectiveness of applying surface-curvature analysis to characterize these trends over regions of the ice sheet [Rémy and Minster, 1997; Le Brocq et al., 2008]. Hence, we assessed the variability of the MODIS imagery to map ESH by applying the ArcGIS 'Raster Curvature' function to the 125 m resolution MOA surface morphology image map [Haran et al., 2006]. The Raster Curvature function calculates the second derivative (i.e. the slope of the slope) of a surface (in this case the MODIS MOA image) on a cell-by-cell basis [Kimerling et al., 2011]. The first derivative converts regional trends in the image to a simple level offset, whilst the second derivative converts all level offsets to zero. Areas with the most variable surface imagery, and likely thin ice, are therefore revealed as regions with high or low second derivative values (>0.05, or <-0.05). Three outputs are generated by the 'Raster Curvature' function: (i) profile curvature - the curvature of the surface parallel to the direction of the maximum slope; (ii) plan curvature - the curvature of the surface perpendicular to the direction of the maximum slope; and (iii) curvature - the overall curvature of a surface, i.e. the combination of the profile and plan curvature. For our data, the profile curvature proved to be the most useful for investigating our area of interest (i.e ESH). For profile curvature, at any given cell location, a negative value indicates that the surface is upwardly convex at that point, a positive value indicates the surface to be upwardly concave, whilst a value of zero indicates a linear surface.

3 RESULTS

3.1 RADIO-ECHO SOUNDING OF THE ELLSWORTH TROUGH

The geomorphology of ET and its surrounding area is diagnostic of a well-developed glaciated valley network. This section describes the geomorphology of the ET from RES data acquired over the northwestern (high-resolution ground-based data) and southeastern (airborne data) ends of the trough (Figures 2 and 3).

In the northwestern parts of the trough (Figures 1 and 2), ET has a relief exceeding 2500 m, contains ice in excess of 3200 m thick, is up to 7 km wide and is classically U-shaped (Figure 3a). Towards the present-day Amundsen-Weddell ice divide, in the south-eastern parts of the ground-based survey, the base of ET is characterized by subdued relief (800-1000 m bsl) and valley-floor morphology for nearly 30 km (Figure 3b).

Approximately 6 km up-ice of ESL the trough floor begins to deepen, with a steep slope down to the lake margin at ~1200 m bsl. ESL lies within the ET in a ~15-20 km-long overdeepened basin. Seismic reflection data [Woodward et al., 2010] show the lake floor reaches a minimum elevation of 1393 ± 10 m bsl, ~400 m below the average elevation of the upper trough (Figures 3a and 3b). The rock-sediment interface of the over-deepening must lie below the minimum elevation of the lake bed observed in the seismic data, however, because acoustic impedance analysis suggests that the lake bed is a water/sediment boundary [Woodward et al., 2010; Siegert et al., 2012]. Down-ice, towards the northwest, the trough bed (i.e. the base of the lake) rises sharply to a prominent ridge, which currently impounds ESL. Roughly orthogonal to present-day ice flow, the ridge (ESLR), ~1.5 km wide, lies at an oblique angle across the entire width (~7 km) of the valley. At an elevation of ~835 m bsl, the ridge crest is ~200 m above the elevation of the down-ice lake margin and at least 550 m above the base of the overdeepening (Figure 3b). Immediately down-ice of the ridge is a narrow linear depression (5 km x 0.75 km) (Figure 3a and 3b), oriented parallel to the ridge, beyond which the bed elevation rises (Figure 3b). ET broadens down-ice of the lake and the impounding ridge (Figure 3a).

Prominent steep-sided bedrock walls confine both sides of the northwestern parts of ET along the majority of its length (Figure 3a). These valley sidewalls contain a number of deep tributary ‘hanging’ valleys, oriented roughly orthogonal to the main trough axis and present-day ice flow. The hanging valleys have a smooth concave, U-shaped cross-profile (Figure 4). They are significant features; the largest is ~3 km across (ridge-crest-to-ridge-crest) and ~1 km deep, with a valley floor perched >1 km above the floor of ET, at an elevation of -100 to 0 m bsl. The 3D form of these features, suggested by the gridded bed (Figure 3a), is not an artifact of the interpolation procedure; in many cases individual hanging valleys are either observed in more than one parallel survey line, or orthogonal survey lines intersect above the valley axis. Most of the hanging valleys aligning ET are confluent with, or just up-valley of, the main trough overdeepening which contains Lake Ellsworth (Figure 3a), consistent with glaciological theory and observations [Linton, 1963; Crabtree, 1981].

Aerogeophysical data acquired over the upper catchments of IIS and MIS have also allowed us to characterize the subglacial topography of the southeastern end of the Ellsworth Trough (Figures 1 and 2). ET is one of three major valleys, ET, T1 and T2 (T2 = Horseshoe Valley), (Figure 3c) which enter the deep subglacial basin beneath IIS [Ross et al., 2012]. ET is the widest and deepest of these valleys, however, at >30 km across, and, at the deepest point that we were able to measure, >2 km deep. Ice thickness over some parts of the southeastern ET exceeds 3000 m. Like the northwestern end of the trough, mountainous topography lines both sides of the southeastern ET. Such topography is most prominent to the northeast of the trough (between ET and T1) where an elongated ridge, 0-500 m above sea level, and characterized by numerous hanging valleys, mountain peaks and ridges is found (see section 3.2 and Figure 9). In some of the deepest parts of the trough (e.g. Figure 9b), the higher-frequency airborne radar was unable to image the trough floor, although the overall form of the southeastern ET is generally well characterized. Our data suggest that the valley floor of the southeastern ET comprises a series of basins, separated by rock bars (Figure 3c). An upper basin (UB) (60 km long and 1500-1700 m below sea level) is separated from a lower basin (LB) (30 km long and 1500-2100 m below sea level) by a prominent, but dissected, ridge (R1) 1200-1500 m below sea level. The lower basin terminates at a broad (25 km) area of higher relief (R2) (1000-1500 below sea level) which lies across the entire width (~35 km) of the valley (Figures 3c and 3d). Like the ridge that terminates the overdeepening associated with ESL in the northwestern ET (ESLR), R2 is located where the trough broadens down-ice as it enters a deep subglacial basin. The southeastern sector of the ET is an enhanced flow tributary of IIS. Present-day ice flow through the southeastern parts of ET, over UB, R1, LB and R2, ranges between 50-75 m a^{-1} [Rignot et al., 2011] (Figure 2c). Down-ice of R2 the basal topography falls away again (>2000 m below sea level) (Figures 3c and 3d) and ice velocity increases markedly, exceeding 125 m a^{-1} 25 km down-ice of the ridge [Rignot et al., 2011].

3.2 MAPPING THE ELLSWORTH SUBGLACIAL HIGHLANDS WITH SATELLITE IMAGERY

In this section, we use MODIS MOA ice surface imagery to demonstrate that the northwestern and southeastern ends of the ET, as described above, are directly connected as a deep subglacial valley across the entirety of the ESH mountain range. We also demonstrate that the ET may only be one of several similar troughs within the ESH.

Comparing subglacial geomorphology with MODIS MOA surface imagery (as outlined in Section 2), a striking correlation between the basal topography and the relative texture of the ice surface is apparent (Figure 5). The deep ET, as mapped by RES surveys, corresponds with a distinct 'smooth' ice surface (i.e. there is little localized spatial variability in MODIS MOA ice surface imagery) (Figures 5a and 5b), whilst the surrounding subglacial mountains are associated with a discrete 'rough' ice surface (i.e. there is significant and high-amplitude localized spatial variability in MODIS ice surface imagery). We are not the first to suggest a relationship between satellite imagery of the ice sheet surface and the form of the subglacial bed [see Crabtree, 1981; Denton et al., 1992; Jezek, 1999] but our high-resolution mapping of the northwestern end of ET enables us to confirm the close relationship between the two. The contrast in texture is believed to be caused by a combination of ice flow over bedrock bumps [Gudmundsson 2003; Smith et al., 2006] and differential surface accumulation [Welch and Jacobel, 2005] associated with marked and abrupt variations in the relief of basal topography (i.e. between deep valleys and rugged high-relief uplands). Profile curvature analysis of the MODIS MOA imagery over and around ET clearly emphasizes the major subglacial geomorphic features of interest (Figure 5c).

The profile curvature analysis of the MODIS ice surface imagery clearly shows that the northwestern and southeastern parts of ET are directly connected (Figure 2), marking out ET as a glacial breach which cuts through the entire ESH. This suggestion is supported by along-track bed elevation measurements acquired by other surveys beyond those parts of the trough that we surveyed [Vaughan et al., 2006; A. Rivera *unpublished data*]; all existing evidence is consistent with a long, deep subglacial trough which breaches the mountain range.

The relationship between the high-resolution basal topography of ET and the MODIS MOA ice surface imagery can be extrapolated to allow the geomorphology of large parts of ESH to be inferred (Figure 6a-c). The correlation between the profile curvature map derived from the MODIS imagery and the bed topography is also strong in other subglacial highland areas of West Antarctica where good bed topography data exist (e.g. in parts of Marie Byrd Land) [Blankenship et al., 2001]), providing confidence in the use of the MODIS MOA profile curvature map as a proxy for inferring the planform of the bed topography across the entire ESH in regions where RES data are uncommon (Figure 6c). Because the broader topography of ESH is not known in detail, ET is currently the only subglacial valley that can be confidently proposed as a deep glacial breach through the entire range. Based on the profile curvature analysis of the MODIS MOA imagery, however, we hypothesize that a number of deep broad glacial troughs, many previously unmapped, and lined by numerous orthogonally-oriented hanging tributary valleys, are present throughout the entire ESH (Figure 6c). A series of major troughs lie between the western flank of the Sentinel Range and ET. Some of these troughs, highlighted previously by King [2009], drain Ellsworth Mountains ice northward into the Rutford Ice Stream and have clear trough heads [Linton, 1963]. From the MODIS imagery we recognise a series of other, previously unreported or little documented troughs within ESH (Figure 6c). Our analysis suggests that at least three further troughs (T1, T3, T4 and possibly T5) may breach the entire ESH massif in a manner similar to ET (Figure 6c). A very narrow trough, which reaches a depth of 1295 m bsl [see seismic station 630 of the Sentinel Mountains Traverse of Bentley and Ostenso, 1961], is located between ET and the Heritage Range of the Ellsworth Mountains (Figures 2 and 6c), and truncates the cirque-headed valleys which adorn the western flanks of these mountains. The MODIS MOA data suggests that this narrow trough likely connects directly with 'T1' in Figure 3c. Two further troughs (T3 and T4) are located further west than the ET, on either side of the Martin-Nash Hills subglacial massif [Drewry and Jordan, 1983; Garrett et al., 1988; Ross et al., 2012; Jordan et al., 2013] (Figure 7). T3 is a major trough incised deeply between the Whitmore Mountains and Mounts Woollard/Moore [Drewry and Jordan, 1983; Garrett et al., 1988]. T3, T4, ET and a sixth large trough (T5) are associated with zones of ice surface 'drawdown', manifested as a series of ice-surface 'saddles' along the axis of the Amundsen-Weddell and Weddell-Ross sections of the primary WAIS divide (Figure 7a). MODIS MOA imagery reveals significant geomorphic detail, not apparent from along-track RES data, demonstrating that these major troughs are associated with a complex of dendritic, transection tributary valleys, particularly to the south of the nunataks of Mount Woollard and Mount Moore (Figure 7b).

Careful examination of MODIS MOA imagery elsewhere across the ESH reveals similarly detailed glacial geomorphic information additional to that revealed by RES data. The Pirrit Hills are the subaerial representation of a large subglacial massif which lies to the west of ET beneath IIS catchment (Figure 8). Radar data show that the Pirrit Hills massif, which is predominantly composed of Jurassic granite [Storey et al., 1988; Jordan et al., 2013], has been highly dissected by glacial erosion (Figure 8b). To the north of the subglacial massif, beyond the high-resolution, gridded part of our aerogeophysical survey (Figures 1 and 3), the MODIS imagery reveals a subglacial valley complex, comprising a deep central basin and a series of radial tributary valleys (Figure 8a). The central basin hosts a limb of the present-day ET enhanced flow tributary of the IIS (Figure 8a). The planform of the valley complex is dendritic, reflecting a pre-glacial period of fluvially-dominated landscape evolution. During later periods of restricted glaciation, however, (i.e. when ESH supported an ice cap or ice field) these valleys would play an important role in controlling the direction of ice flow, draining ice into the southeastern part of ET.

Across the ET from the Pirrit Hills, to the northeast of the ET and the enhanced flow tributary of the IIS (Figure 2c), we identify a series of ice surface features, orthogonal to present-day ice flow, on the northeastern flanks of the ET (Figure 9a). The MODIS MOA imagery reveals these features to be a complex of near-ice-surface subglacial hanging valleys, separated by prominent spurs and arêtes, adorning a 100 km-long, linear subglacial mountain ridge composed of a mixture of Cambrian-Permian meta-sediments and Cambrian volcanics [Jordan et al., 2013] (Figure 9). The form and spacing of these landforms is directly comparable to subaerial hanging valleys and spurs observed on the western flanks of the Sentinel Range, reinforcing our interpretation that the ice surface features we observe and identify from the MODIS MOA, and from the profile curvature analysis of the MOSAIC, are representative of the subglacial geomorphology beneath.

4 THE ELLSWORTH SUBGLACIAL HIGHLAND ICE FIELD

At its maximum ET is ~325 km long and more than 25 km wide (Figure 2); comparable in scale and dimensions to the troughs beneath Byrd Glacier and Beardmore Glacier in East Antarctica [Stearns et al., 2008; Denton et al., 1989], and Jakobshavn Isbrae in western Greenland [Peters, et al., 2012]. Understanding the geomorphology of ET is key to reconstructing the configuration of the paleo- ice mass(es) responsible for its formation.

The subglacial landforms associated with ET (hanging tributary valleys, valley steps, valley overdeepenings rising to prominent ridges, and down-ice-flow valley widening) are consistent with the geomorphology of a glacially-carved fjord [e.g. Holtedahl, 1967]. The ridges are particularly indicative; bedrock ridges often form in fjord-mouths because of a sudden decrease in the erosive capacity. This decrease is due to: (i) a shift to a divergent ice flow regime, caused by the sudden lack of lateral constraint from valley sidewalls at the valley mouth [Holtedahl, 1967; Shoemaker 1986]; and (ii) the glacier approaching floatation near its tidewater-terminating margin [Crary, 1966]. The reduction in basal erosion rates leads to an abrupt termination to the valley overdeepening and the formation of the threshold. The ridges identified at both the northwestern and southeastern ends of ET (ESLR and R2) are located across the entire width of the valley at the down-ice end of significant overdeepenings at points where the valley widens down-ice and are therefore interpreted as fjord-mouth threshold bars (Figure 3). The location of overdeepenings immediately down-ice of tributary valley confluences (e.g. in the northwestern part of ET) is consistent with normal fjord geometry and a convergent ice flow regime [Crabtree, 1981], whilst subglacial erosion by meltwater, such as might be represented by a possible channel incised into the northwestern threshold bar (ESLR), is also well documented within fjords [Holtedahl, 1967]. Hence, ET represents evidence of former highly-erosive dynamic glaciers, terminating into water at valley mouths.

The overdeepenings (at least one of which is asymmetric in profile) with threshold bars at both ends of ET suggests that the trough was cut by an ice mass centered over ESH, rather than by the advancing margin of an ice sheet impeded by the rock barrier of ESH. As such, the broad-scale mechanism for the formation of ET is different from that proposed for large troughs in East Antarctica [Young et al., 2011] and the Transantarctic Mountains [Sugden and Denton, 2004], although the primary process (glacial erosion) is the same. Instead, trough incision took place when restricted ice masses occupied ESH. We reject the idea that the overdeepenings and threshold bars were formed beneath present-day ice-sheet conditions; the rate of ice flow over the vast majority of ESH, in the interior of the ice sheet, is slow (<25 ma^{-1}) [Ross et al., 2011; Rignot et al., 2011], prohibiting significant recent basal erosion. Furthermore, the formation of the landform assemblage surrounding the trough (i.e. rugged mountainous topography with hanging tributary valleys) is entirely incompatible with the present-day cold-based regime of the thinner parts of the ice sheet; deep, U-shaped hanging tributary valleys incised to elevations around present-day sea level (e.g. Figure 4) require warm-based conditions for their formation.

Glacial troughs and fjords breaching massifs along structural weaknesses and sometimes across pre-existing fluvial valleys have long been recognized as diagnostic features of glacial erosion by ice sheets (e.g. in Scotland, North America, Norway, Greenland and Chile) [Holtedahl, 1967; Sugden 1968, 1974, 1978; Nesje and Whillans, 1994; Glasser and Ghiglione, 2009]. The northwest to southeast orientation of the ET, and other immediately-adjacent subglacial troughs, parallels the dominant structural grain of the Ellsworth Mountains, where fold axial planes in Cambrian-Permian meta-sediments are aligned northwest to southeast [Craddock et al., 1992; Spörli et al., 1992; Curtis, 2001]. Prominent magnetic lineaments over the Ellsworth Mountains have also recently been interpreted as revealing northwest to southeast oriented basement faults [Jordan et al., 2013]. ET and the other ESH troughs are therefore likely to have been formed by an ice mass exploiting and eroding these pre-existing structural weaknesses (i.e. through 'selective linear erosion') [c.f. Bingham et al., 2012].

The form of ET, the prominent overdeepenings and the hanging valleys are all diagnostic of a dynamic alpine glaciated valley environment associated with a predominantly maritime climate. The troughs must have formed when the marine sections of the WAIS were largely absent (either prior to WAIS development or during a 'collapse' event), when small ice fields occupied the topographic highlands of the region, confirming previous hypotheses about WAIS initiation and decay [Bentley et al., 1960; Bamber et al. 2009; DeConto and Pollard, 2003]. On such occasions, with global ice volumes below present-day levels and without West Antarctic isostatic depression, the present-day Bentley Subglacial Trench would have been a deep marine basin, with a coastline along the edge of the present-day ESH. To the southeast, the deep marine basins underlying IIS and MIS [Janowski and Drewry 1981; Ross et al., 2012] would also have been inundated. The former glacier within ET is therefore likely to have terminated as a tidewater glacier, consistent with our interpretation of the bedrock ridges identified in RES data as fjord-mouth threshold bars, and the margin of the associated grounded ice field well-defined at the flanks of ESH. The asymmetry of the overdeepenings (Figure 3) and the planform of the tributary complex northwest of the Pirrit Hills (Figure 8a) suggest that the flow of this ice field was separated by a primary divide located over the axis of ESH, near to, and with a similar orientation to, the present-day Amundsen-Weddell divide (Figure 7) [Ross et al., 2011].

We have no direct dates on the landforms of ESH so we cannot determine a robust age for trough formation and the dissection of ESH. The landscape is clearly a composite one, however, having formed during a series of alpine glaciations over the last 34 Ma through a combination of glacial and sub-aerial (erosion) processes when the marine ice sheet was absent. Subglacial evidence [Scherer et al., 1998] and far-field sea level data [e.g. Raymo and Mitrovica, 2012], support a restricted WAIS during MIS11 (420-360 ka), but the duration of this interglacial (<60 ka) was too short to allow the incision of >1 km deep troughs into the predominantly metasedimentary bedrock of ESH at that time [Kessler et al., 2008]. Instead, it is likely that the most recent significant erosion of ESH occurred during the Early Pliocene [4.6-3.3 Ma], when the marine sections of the WAIS were significantly diminished [McKay et al., 2012].

Unlike major former ice sheet changes in East Antarctica, that would require substantial alteration to climate and ocean conditions to occur [e.g. Bo et al., 2009], restricted ice caps in West Antarctica may well be consistent with the present climate if the current ice mass were to decay. For example, the Antarctic Peninsula, to the immediate north of ESH, currently contains several modest-sized ice caps (e.g. Dyer Plateau, Avery Plateau) that cover subglacial highlands and terminate in water. Deep fjord structures, with overdeepened basins and steps, and which follow geological structure, underlie, or have underlain, the outlet glaciers of these ice caps [Crabtree 1981; Scambos et al., 2011].

CONCLUSIONS

We have: (i) characterized the detailed subglacial morphology (u-shaped troughs, hanging tributary valleys, valley overdeepenings, and threshold sills) of the Ellsworth Subglacial Highlands (ESH), West Antarctica; (ii) identified and mapped a series of deep subglacial troughs, one of which, the Ellsworth Trough, is >25 km across >300 km long, and is incised into, and breaches, the ESH; (iii) reconstructed the glaciology and flow regime of the ice mass responsible for the form of the ESH, to show that the subglacial landscape was cut by a small, dynamic, highly-erosive, warm-based, marine-proximal icefield, characterized by tidewater (fjord-mouth) margins; (iv) demonstrated the considerable potential provided by the application and analysis of satellite remote sensing imagery of the ice sheet surface for the mapping of subglacial topography.

Our findings support the proposition that, in the absence of a large-scale marine ice-sheet, small dynamic ice caps or ice fields characterized, at least in part, by tidewater margins, are likely to be centred on the prominent highlands in West Antarctica [Bentley et al., 1960; DeConto and Pollard 2003; Pollard and DeConto 2009]. These ice masses, similar in character and dynamics to those of the present-day Antarctic Peninsula, play a key role in the seeding and early growth of the marine based sectors of the WAIS and in the stabilisation of retreating marine-based West Antarctic Ice Sheets [Bentley et al., 1960; Weertman et al., 1974; Bamber et al., 2009].

ACKNOWLEDGEMENTS

Financial support was provided by the UK Natural Environment Research Council (NERC) Antarctic Funding Initiative (AFI) grants NE/G013071/1 and NE/D008638/1. The NERC Geophysical Equipment Facility provided GPS equipment (loans 838, 870). We thank the British Antarctic Survey for logistics support, J. Woodward, A. Smith, E. King, R. Hindmarsh and D. Vaughan for assistance in the planning and acquisition of DELORES data from Lake Ellsworth, M. Bentley and D. Sugden for discussion of an earlier draft of this manuscript, A. Rivera for sharing unpublished radar data, and M. LeCompte for advice on remote sensing imagery. D. Fitzgerald, D. Routledge, C. Robinson, I. Potten, D. Cochrane and M. Oostlander are thanked for their invaluable support in the field. Two reviewers and an Associate Editor are thanked for insightful comments that significantly improved the manuscript. We would also like to acknowledge the hard work done by the MODIS MOA team in compiling the MOA imagery. Without it, this work would not have been possible.

REFERENCE LIST

Bamber, J.L., Riva, R.E.M., Vermeersen, B.L.A., and LeBrocq, A.M., 2009, Reassessment of the potential sea-level rise from a collapse of the West Antarctic Ice Sheet: Science, v. 324, p. 901-903.

Bamber, J.L., Gomez-Dans, J.L., and Griggs, J.A., 2009, *Antarctic 1 km Digital Elevation Model (DEM) from Combined ERS-1 Radar and ICESat Laser Satellite Altimetry*. Boulder, Colorado USA: National Snow and Ice Data Center. Digital media.

Bell, R.E., Ferraccioli, F., Creyts, T.T., Braaten, D., Corr, H., Das, I., Damaske, D., Frearson N., Jordan, T., Rose, K., Studinger, M., and Wolovick, M., 2011, Widespread persistent thickening of the East Antarctic Ice Sheet by freezing from the base: Science, v. 331, p. 1592-1595.

Bentley, C.R., Crary, A.P., Ostenso, N.A., and Thiel, E.C., 1960, Structure of West Antarctica: Science, v. 131, p. 131-136.

Bentley, C., and Ostenso, N.A., 1961, Glacial and subglacial topography of West Antarctica: Journal of Glaciology, v. 29, p. 882-912.

Bentley, M.J., 2010, The Antarctic palaeo record and its role in improving predictions of future Antarctic Ice Sheet change: Journal of Quaternary Science, v. 25, p. 5-18.

Bingham, R.G., Ferraccioli, F. , King, E.C. , Larter, R.D. , Pritchard, H.D., Smith, A.M., and Vaughan, D.G., 2012, Inland thinning of West Antarctic Ice Sheet steered along subglacial rifts: Nature, v. 487, p. 468-471.

Blankenship, D.D., Morse, D.L., Finn, C.A., Bell, R.E., Peters, M.E., Kempf, S.E., Hodge, S.M., Studinger, M., Behrendt, J.C., and Brozena, J.M., 2001, Geologic controls on the initiation of rapid basal motion for the West Antarctic ice streams: a geophysical perspective including new airborne radar sounding and laser altimetry results. In: Alley, R.B., Bindschadler, R.A., (eds) The West Antarctic Ice Sheet: behavior and environment. Antarctic Research Series 77, AGU, Washington DC, pp 283-296.

Bo, S., Siegert, M.J., Mudd, S.M., Sugden, D., Fujita, S., Xiangbin, C., Younyou, J., Xueyuan, T., and Yuansheng, L., 2009, The Gamburtsev mountains and the origin and early evolution of the Antarctic Ice Sheet: Nature, v. 459, p. 690-693.

Corr, H., Ferraccioli, F., Frearson, N., Jordan, T., Robinson, C., Armadillo, E., Caneva, G. Bozzo, E., and Tabacco, I., 2007, Airborne radio-echo sounding of the Wilkes Subglacial Basin, the Transantarctic Mountains, and the Dome C region: Terra Antartica Reports, v. 13, p. 55-64.

Crabtree, R.D., 1981, Subglacial morphology in northern Palmer Land, Antarctic Peninsula: Annals of Glaciology, v. 2, p. 17-22.

Craddock, C., Spörli, K.B. and Anderson, J.J. 1992, "Structure of the Sentinel Range, Ellsworth Mountains, West Antarctica; Geology and paleontology of the Ellsworth Mountains, West Antarctica", Memoir - Geological Society of America, vol. 170, pp. 393-402.

Crary, A.P., 1966, Mechanism for Fiord formation indicated by studies of an ice-covered inlet: Geological Society of America Bulletin, v. 77, p. 911-930.

Curtis, M.L., 2001, Tectonic history of the Ellsworth Mountains, West Antarctica: reconciling a Gondwana enigma: Geological Society of America Bulletin, v. 113, p. 939-958.

DeConto, R.M., and Pollard, D., 2003, Rapid Cenozoic glaciation of Antarctica induced by declining atmospheric CO2: Nature, v. 421, p. 245-249.

Denton, G.H., Bockheim, J.G., Rutford, R.H., and Andersen, B.G., 1992, Glacial History of the Ellsworth Mountains, West Antarctica. In: Webers, G.F., Craddock, C., and Splettstoesser, J.F., eds., Geology and Palaeontology of the Ellsworth Mountains, West Antarctica: Boulder, Colorado, Geological Society of America Memoir 170, pp 403-432.

Denton, G.H., Bockheim, J.G., Wilson, S.C., Leide, J.E., and Andersen, B.G., 1989, Late Quaternary ice-surface fluctuations of Beardmore Glacier, Transantarctic Mountains: Quaternary Research, v. 31, p. 183-209.

DiMarzio, J., Brenner, A., Fricker, H., Schutz, R., Shuman, C. A., and Zwally, H. J., 2007, *GLAS/ICESat 500 m laser altimetry digital elevation model of Antarctica*. Boulder, Colorado USA: National Snow and Ice Data Center. Digital media.

Drewry, D.J., and Jordan, S.R., 1983, The bedrock surface of Antarctica, in *Antarctica: Glaciological and Geophysical Folio*, Scott Polar Research Institute, Cambridge, England.

Ferraccioli, F., Finn, C.A., Jordan, T.A., Bell, R.E., Anderson, L.M., and Damaske, D., 2011, East Antarctic rifting triggers uplift of the Gamburtsev Mountains: Nature, v. 479, p. 388-394.

Fretwell, P., Pritchard, H.D., Vaughan, D.G., Bamber, J.L., Barrand, N.E., Bell, R., Bianchi, C., Bingham, R.G., Blankenship, D.D., Casassa, G., Catania, G., Callens, D., Conway, H., Cook, A.J., Corr, H.F.J., Damaske, D., Damm, V., Ferraccioli, F., Forsberg, R., Fujita, S., Gim, Y., Gogineni, P., Griggs, J.A., Hindmarsh, R.C.A., Holmlund, P., Holt, J.W., Jacobel, R.W., Jenkins, A., Jokat, W., Jordan, T., King, E.C., Kohler, J., Krabill, W., Riger-Kusk, M., Langley, K.A., Leitchenkov, G., Leuschen, C., Luyendyk, B.P., Matsuoka, K., Mouginot, J., Nitsche, F.O., Nogi, Y., Nost, O.A., Popov, S.V., Rignot, E., Rippin, D.M., Rivera, A., Roberts, J., Ross, N., Siegert, M.J., Smith, A.M., Steinhage, D., Studinger, M., Sun, B., Tinto, B.K., Welch, B.C., Wilson, D., Young, D.A., Xiangbin, C., Zirizzotti, A., 2013, Bedmap2: improved ice bed, surface and thickness datasets for Antarctica: The Cryosphere, v. 7, p. 375-393.

Garrett, S.W., Maslanyj, M.P., and Damaske, D., 1988, Interpretation of aeromagnetic data from the Ellsworth Mountains-Thiel ridge, West Antarctica: Journal of the Geological Society, London, v. 145, p. 1009-1017.

Glasser, N.F., and Ghiglione, M.C., 2009, Structural, tectonic and glaciological controls on the evolution of fjord landscapes: Geomorphology, v. 105, p. 291-302.

Gudmundsson, G.H., 2003, Transmission of basal variability to a glacier surface: Journal of Geophysical Research, v. 108, 2253, doi:10.1029/2002JB002107.

Haran, T., Bohlander, J., Scambos, T., Painter, T., and Fahnestock, M. 2005, updated 2006, *MODIS mosaic of Antarctica (MOA) image map*. Boulder, Colorado USA: National Snow and Ice Data Center. Digital media.

Holtedahl, H., 1967, Notes on the formation of fjords and fjord-valleys. Geografiska Annaler Series A, v. 49, p. 188-203.

Janowski, E.J., and Drewry, D.J., 1981, The structure of West Antarctica from geophysical studies: Nature, v. 291, p. 17-21.

Jezek, K.C., 1999, Glaciological properties of the Antarctic ice sheet from RADARSAT-1 synthetic aperture radar imagery: Annals of Glaciology, v. 29, p. 286-290.

Jordan, T.A., Ferraccioli, F., Ross, N., Siegert, M.J., Corr, H.F.J., Leat, P.T., Bingham, R.G., Rippin, D.M., and Le Brocq, A., (2013). Inland extent of the Weddell Sea Rift imaged by new aerogeophysical data: Tectonophysics, v. 585, p. 137-160

Joughin, I., and Alley, R.B., 2011, Stability of the West Antarctic ice sheet in a warming world: Nature Geoscience, v. 4, p. 506-513.

Joughin, I., Bamber, J.L., Scambos, T., Tulaczyk, S., Fahnestock, M., and MacAyeal, D.R., 2006, Integrating satellite observations with modelling: basal shear stress of the Filchner-Ronne ice streams, Antarctica: Philosophical Transactions of the Royal Society A, v. 364, p. 1795-1814.

Karlsson, N.B., Rippin, D.M., Bingham, R.G. and Vaughan, D.G., 2012, Determination of a “continuity-index” for assessing ice-sheet dynamics from radar-sounded internal layers: Earth and Planetary Science Letters, v. 335-336, p. 88-94.

Kessler, M.A., Anderson, R.S., and Briner, J.P., 2008, Fjord insertion into continental margins driven by topographic steering of ice: Nature Geoscience, v. 1, p. 365-369.

Kimerling, A.J., Buckley, A.R., Muehrcke, P.C., and Muehrcke, J.O., 2011, Map Use: Reading Analysis Interpretation, ESRI press, pp. 620.

King, E.C., 2009, Flow dynamics of the Rutford Ice Stream ice-drainage basin, West Antarctica, from radar stratigraphy: Annals of Glaciology, v. 50, p. 42-48.

Le Brocq, A.M., Hubbard, A., Bentley, M.J., and Bamber, J.L., 2008, Subglacial topography inferred from ice surface terrain analysis reveals a large un-surveyed basin below sea level in East Antarctica: Geophysical Research Letters, v. 35, L16503, doi:10.1029/2008GL034728.

Linton, D.L., 1963, The forms of glacial erosion: Transactions of the Institute of British Geographers, v. 33, p. 1-28.

McKay, R., Naish, T., Carter, L., Riesselman, C., Dunbar, R., Sjunneskog, C., Winter, D., Sagiorgi, F., Warren, C., Pagani, M., Schouten, S., Willmott, V., Levy, R., DeConto,R., and Powell, R.D., 2012, Antarctic and Southern Ocean influences on Late Pliocene global cooling: Proceedings of the National Academy of Science, v. 109, p. 6423-6428.

Nesje, A., and Whillans, I.M., 1994, Erosion of Sognefjord, Norway: Geomorphology, v. 9, p. 33-45.

Peters, L.E., Anandakrishnan, S., Alley, R.B., and Voight, D.E., 2012, Seismic attenuation in glacial ice: A proxy for englacial temperature: Journal of Geophysical Research, v. 117, F02008, doi:10.1029/2011JF002201

Pollard, D., and DeConto, R.M., 2009, Modelling West Antarctic ice sheet growth and collapse through the past five million years: Nature, v. 458, p. 329-332.

Raymo, M.E., and Mitrovica, J.X., 2012, Collapse of polar ice sheets during the stage 11 interglacial: Nature, v. 483, p. 453-456.

Remy, F., and Minster,J-F., 1997, Antarctic ice sheet curvature and its relation with ice flow and boundary conditions: Geophysical Research Letters, v. 24, p. 1039-1042.

Rignot, E., Mouginot, J., and Scheuchl, B., 2011, Ice flow of the Antarctic Ice Sheet: Science, v. 333, p. 1427-1430.

Ross, N., Bingham, R.G., Corr, H.F.J., Ferraccioli, F., Jordan, T.A., Le Brocq, A., Rippin, D., Young, D., Blankenship, D., and Siegert, M.J., 2012, Weddell Sea sector of the West Antarctic Ice Sheet on the threshold of change: Nature Geoscience, v. 5, p. 393-396.

Ross, N., Siegert, M.J., Woodward, J., Smith, A.M., Corr, H.F.J., Bentley, M.J., Hindmarsh, R.C.A., King, E.C., and Rivera, A., 2011, Holocene stability of the Amundsen-Weddell ice divide, West Antarctica: Geology, v. 39, p. 935-938.

Scambos, T.A., Haran, T.M., Fahnestock, M.A., Painter, T.H., and Bohlander, J., 2007, MODIS-based Mosaic of Antarctica (MOA) data sets: Continent wide surface morphology and snow grain size: Remote Sensing of Environment, v. 111, p. 242-257.

Scambos, T.A., Bethier, E., and Shuman, C.A., 2011, The triggering of subglacial lake drainage during rapid glacier drawdown: Crane Glacier, Antarctic Peninsula: Annals of Glaciology, v. 52, p. 74-82.

Scherer, R.P., Aldahan, A., Tulaczyk, S., Kamb, B., Engelhardt, H., and Possnert, G., 1998, Pleistocene collapse of the West Antarctic Ice Sheet: Science, v. 281, p. 82-85.

Shoemaker, E.M., 1986, The formation of fjord thresholds: Journal of Glaciology, v. 32, p. 65-71.

Spörli, K.B., and Craddock, C., 1992, "Structure of the Heritage Range, Ellsworth Mountains, West Antarctica; Geology and paleontology of the Ellsworth Mountains, West Antarctica", Memoir - Geological Society of America, v. 170, pp. 375-392.

Siegert, M.J., Clarke, R.J., Mowlem, M., Ross, N., Hill, C.S., Tait, A., Hodgson, D., Parnell, J., Tranter, M., Pearce, D., Bentley, M.J., Cockell, C., Tsalogou, M-N, Smith, A., Woodward, J., Brito, M.P., and Waugh, E., 2012, Clean access, measurement and sampling of Ellsworth Subglacial Lake: A method for exploring deep Antarctic subglacial lake environment: Reviews of Geophysics, v. 50, RG1003, doi:10.1029/2011RG000361.

Smith, B.E., Raymond, C.F., and Scambos, T., 2006, Anistrophic texture of ice sheet surfaces: Journal of Geophysical Research, v. 111, F01019, doi:10.1029/2005JF000393

Stearns, L.A., Smith, B.E., and Hamilton, G.S., 2008, Increased flow speed on a large East Antarctic outlet glacier caused by subglacial floods: Nature Geoscience, v. 1, p. 827-831.

Storey, B.C., Hole, M.J., Pankhurst, R.J., Millar, I.L., and Vennum, W., 1988, Middle Jurassic within-plate granites in West Antarctica and their bearing on the break-up of Gondwanaland: Journal of the Geological Society, London, v. 145, p. 999-1007.

Sugden, D.E., 1968, The selectivity of glacial erosion in the Cairngorms Mountains, Scotland: Transactions of the Institute of British Geographers, v. 45, p. 79-92.

Sugden, D.E., 1974, Landscapes of glacial erosion in Greenland and their relationship to ice, topographic and bedrock conditions. In: Waters, R.S., and Brown, E.H., (eds). Progress in geomorphology. Institute of British Geographers Special Publication No. 7, London, pp. 177-195.

Sugden, D.E., 1978, Glacial erosion by the Laurentide ice sheet: Journal of Glaciology, v. 20, p. 367-391.

Sugden, D.E., and Denton, G., 2004, Cenozoic landscape evolution of the Convoy Range to Mackay Glacier area, Transantarctic Mountains: Onshore to offshore synthesis: Geological Society of America Bulletin, v. 116, p. 840-857.

Vaughan, D.G., Corr, H.F.J., Ferraccioli, F., Frearson, N., O'Hare, A., Mach, D., Holt, J.W., Blankenship, D.D., More, D.L., and Young, D.A., 2006, New boundary conditions for the West Antarctic ice sheet: Subglacial topography beneath Pine Island Glacier: Geophysical Research Letters, v. 33, L09501, doi: 10.1029/2005GL025588

Vaughan, D.G., Rivera, A., Woodward, J., Corr, H.F.J., Wendt, J., and Zamora, R., 2007, Topographic and hydrological controls on Subglacial Lake Ellsworth, West Antarctica: Geophysical Research Letters, v. 34, L18501, doi: 10.1029/2007GL030769

Weertman, J., 1974, Stability of the junction of an ice sheet and an ice shelf: Journal of Glaciology, v. 13, p. 3-11.

Welch, B.C., and Jacobel, R.W., 2005; Bedrock topography and wind erosion sites in East Antarctica: observations from the 2002 US-ITASE traverse: Annals of Glaciology, v. 41, p. 92-96.

Woodward, J., Smith, A.M., Ross, N., Thoma, M., Corr, H.F.J., King, E.C., King, M.A., Grosfeld, K., Tranter, M., and Siegert, M.J., 2010, Location for direct access to subglacial Lake Ellsworth: An assessment of geophysical data and modeling: Geophysical Research Letters, v. 37, L11501, doi: 10.1029/2010GL042884.

Young, D.A., Wright, A.P., Roberts, J.L., Warner, R.C., Young, N.W., Greenbaum, J.S., Schroeder, D.M., Holt, J.W., Sugden, D.E., Blankenship, D.D., van Ommen, T.D., and Siegert, M.J., 2011, A dynamic early East Antarctic Ice Sheet suggested by ice-covered fjord landscapes: Nature, v. 474, p. 72-75.

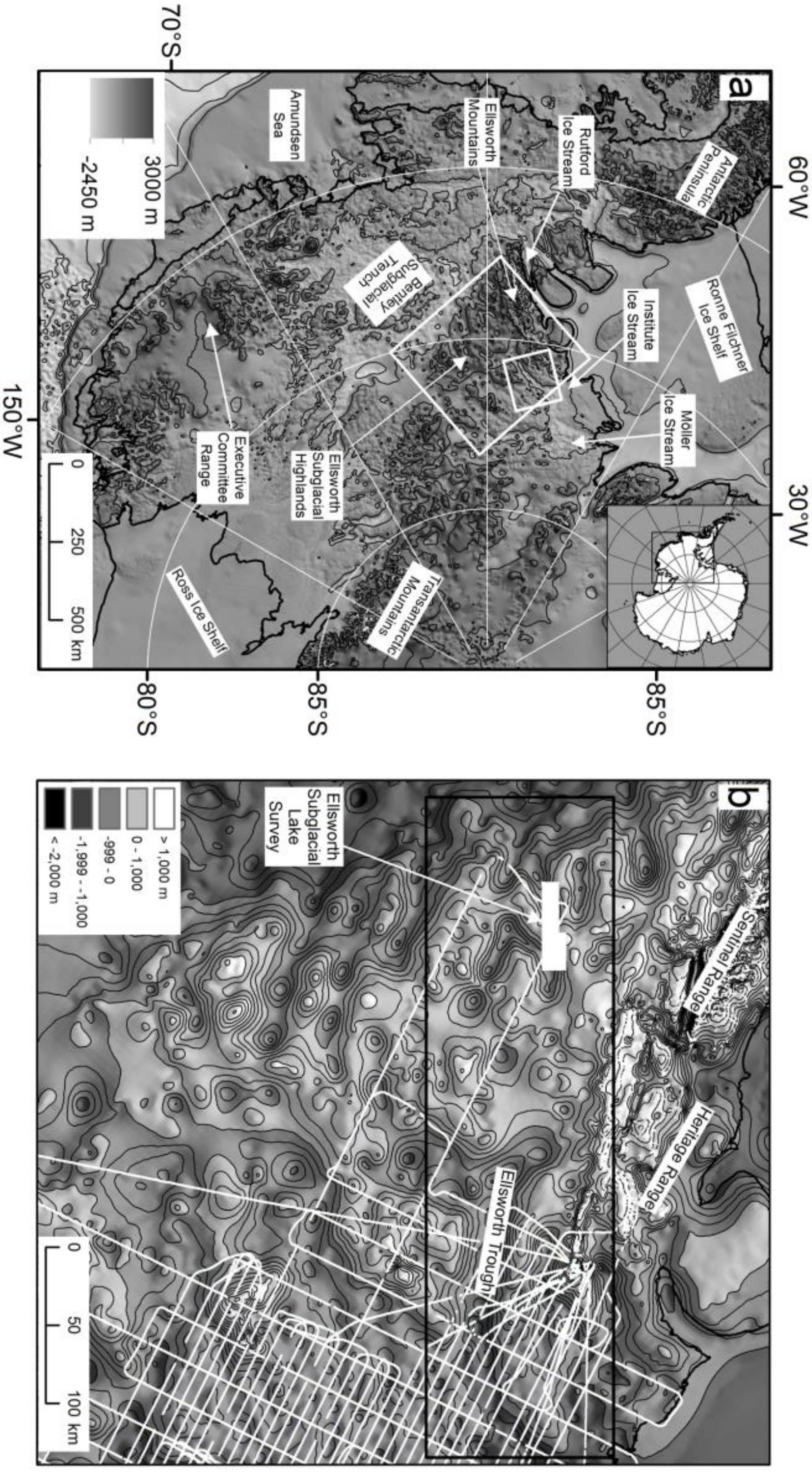
a
70°S
60°W
30°W
150°W
80°S
85°S
85°S
Antarctic Peninsula
Rutford Ice Stream
Ellsworth Mountains
Amundsen Sea
3000 m
-2450 m
Ronne Filchner Ice Shelf
Institute Ice Stream
Bentley Subglacial Trench
Möller Ice Stream
Ellsworth Subglacial Highlands
Executive Committee Range
Transantarctic Mountains
Ross Ice Shelf
0
250
500 km
b
Ellsworth Subglacial Lake Survey
> 1,000 m
0 - 1,000
-999 - 0
-1,999 - -1,000
< -2,000 m
Sentinel Range
Heritage Range
Ellsworth Trough
0
50
100 km

Figure 1: (A) Subglacial topography of West Antarctica (BEDMAP2) (m wgs84) [Fretwell etal., 2013]. Area of Figures 1b, 6a-c, 7a (large white box) and 3c (small white box) shown. Inset shows location of study area. Thin black lines are bed topography contours at 1000 m intervals; (B) Subglacial topography of the Ellsworth Subglacial Highlands (BEDMAP2) (m wgs84) [Fretwell et al., 2013]. Filled white polygons represent areas of exposed bedrock of the Sentinel and Heritage Ranges (from Antarctic Digital Database (ADD)). The white infilled box delimits the area of the 2007-09 ground-based RES survey of Ellsworth Subglacial Lake (figure 3a). Thick white lines show bed elevation measurements made during the 2010-11 aerogeophysical survey of the Institute and Möller Ice Streams. Location of Figure 2 (large black rectangle) shown. Thin black lines are bed topography contours at 250 m intervals.

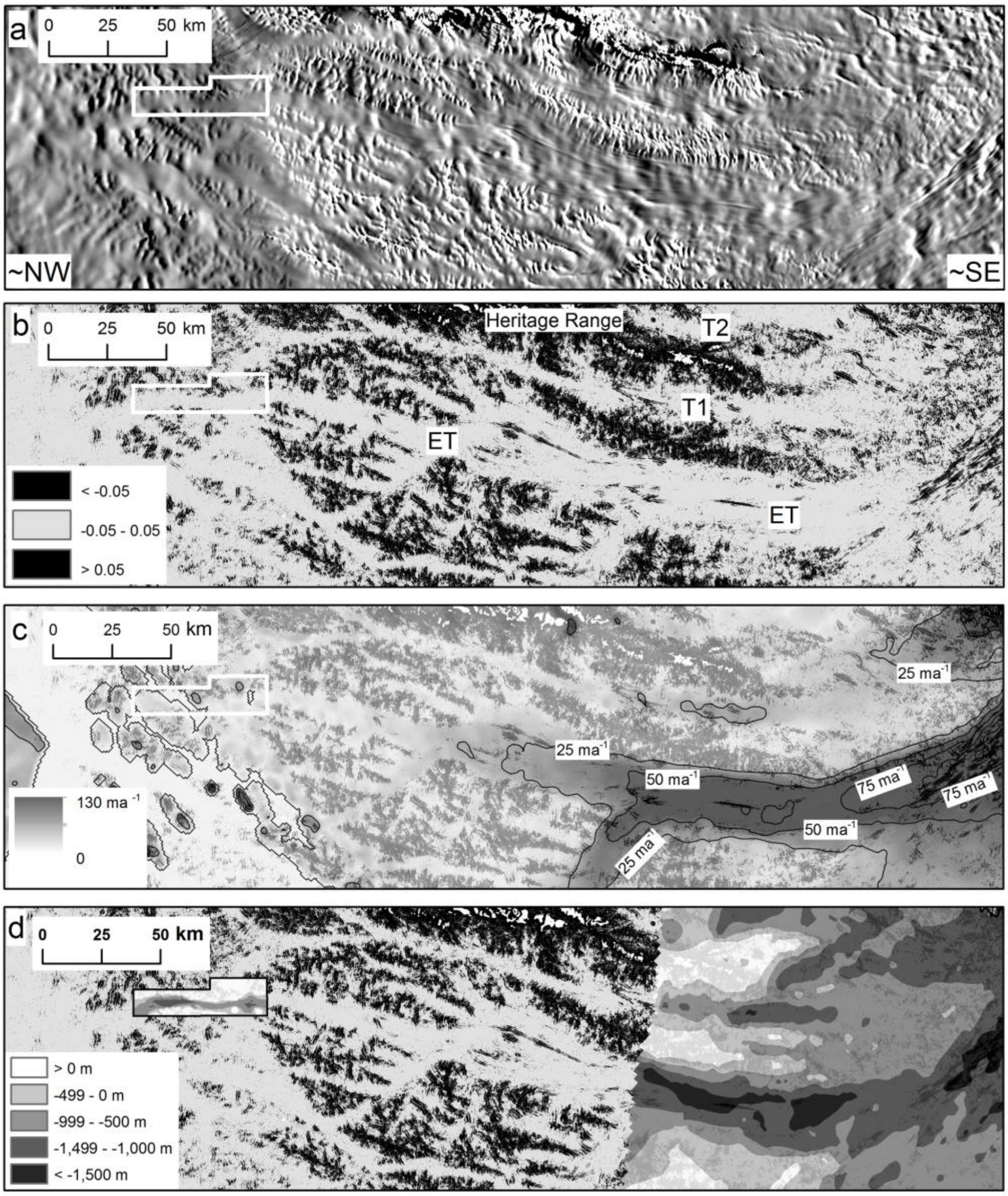

Figure 2: (A) Moderate Resolution Imaging Spectroradiometer (MODIS) Mosaic of Antarctica (MOA) digital image mosaic of the surface morphology of the Antarctic ice sheet [Haran et al., 2006; Scambos et al., 2007] over and around the Ellsworth Trough (ET) (see Figure 1b for location). Small white box (in 2a 2b and 2c) delimits area of ground-based survey around Ellsworth Subglacial Lake. Filled white polygons (in 2a, 2b, 2c and 2d) represent sub-aerially exposed bedrock (from Antarctic Digital Database (ADD)); (B) Profile curvature analysis of MODIS MOA data around the

Ellsworth Trough. Cells with curvature <-0.05 and >0.05 are colored black, cells with curvature between -0.05 and 0.05 are colored light grey; (C) Ice sheet surface velocity [Rignot et al., 2011] superimposed on profile curvature map. Color-scale of velocity data is on a log scale and is saturated at 130 m a^{-1}. Black contours are in 25 m a^{-1} intervals; (D) Bedrock elevation (m wgs 84) from surveys of Ellsworth Subglacial Lake and Institute and Möller ice streams superimposed on map of profile curvature.

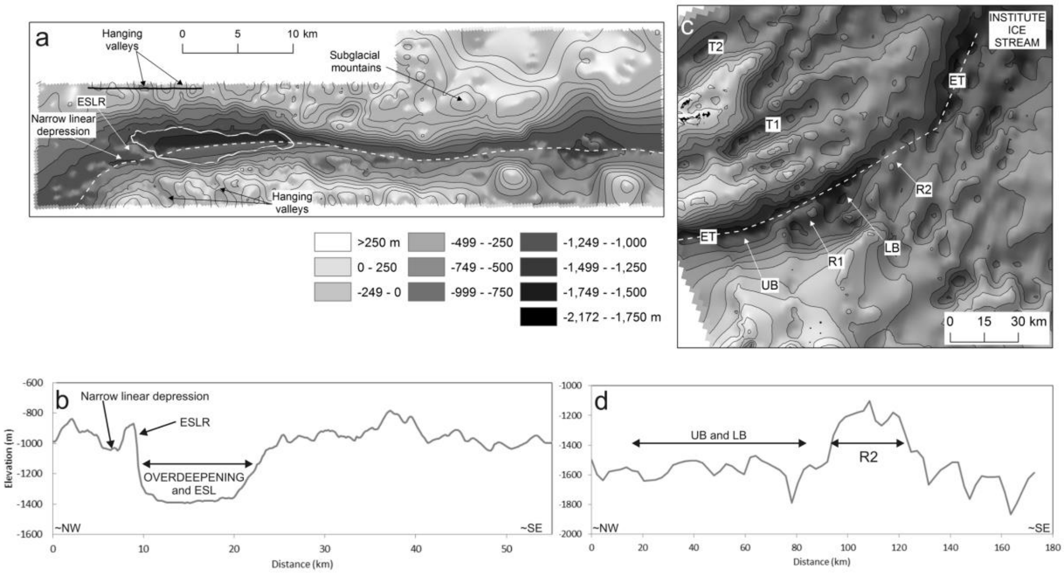

Figure 3: (A) Subglacial topography of the northwestern parts of the Ellsworth Trough from DELORES ground-based radio-echo sounding and seismic reflection data. Contours in 250 m intervals. White dashed line shows location of profile in 3b. Black line is location of Figure 4; (B) Long-axis profile of the subglacial topography of the northwestern parts of the Ellsworth Trough, in the vicinity of Ellsworth Subglacial Lake; (C) Subglacial topography of the southeastern end of the Ellsworth Trough from airborne radio-echo sounding. Contours in 250 m intervals. The three major valleys extending from the Ellsworth Subglacial Highlands are labelled ET, T1 and T2, the two sub-basins of the Ellsworth Trough are labeled UB (upper basin) and LB (lower basin). White dashed line shows location of profile in 3d; (D) Long-axis profile of the subglacial topography of the southeastern parts of the Ellsworth Trough.

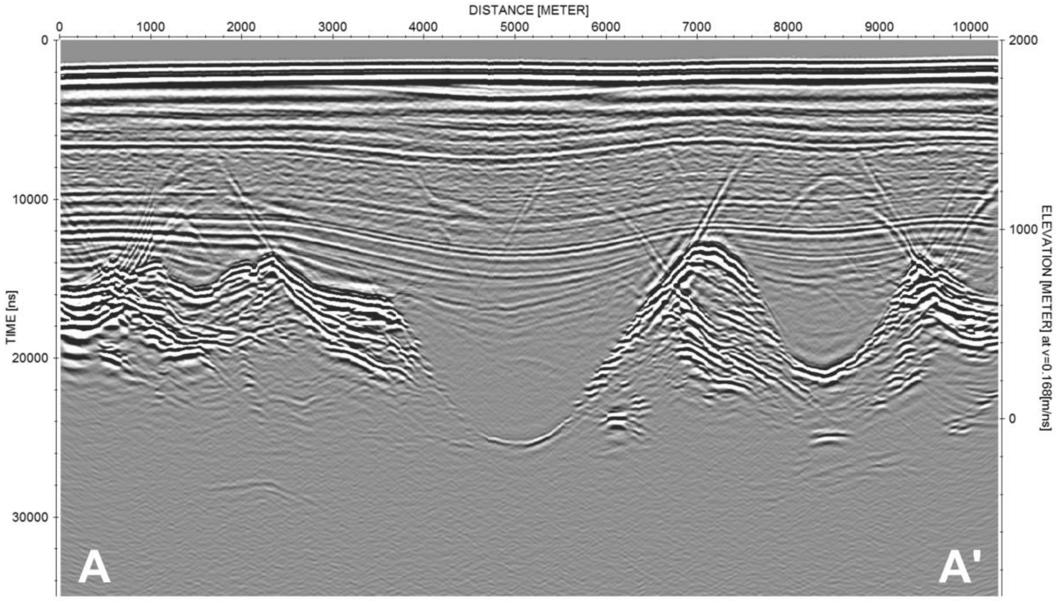

Figure 4: U-shaped hanging tributary valleys of the Ellsworth Trough. The radar survey line is located northeast of the lower parts of the Ellsworth Trough (see Figures 3a and 5a) and runs approximately parallel to the trough and present-day ice flow (which is roughly right to left across radargram). The radargram depicts two obvious tributary valleys, the largest of which is 1 km deep, by 3 km wide. The ice flow responsible for the formation of these features flowed out of the page, i.e. perpendicular to present-day ice flow.

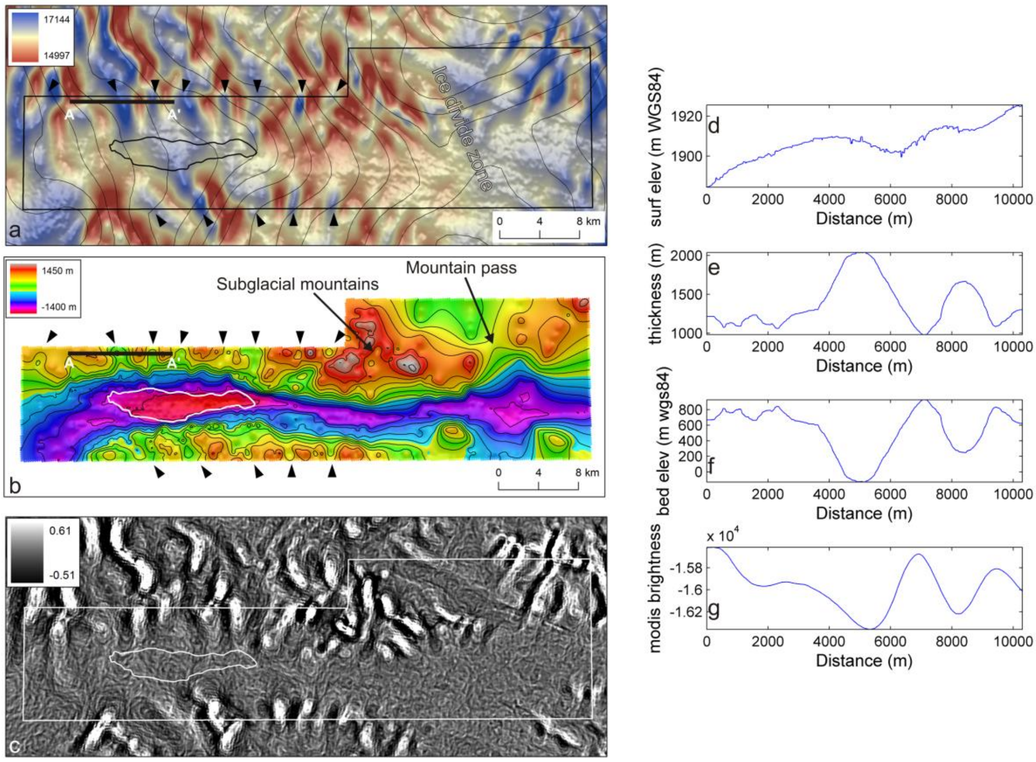

Figure 5 (A) MODIS MOA ice surface imagery of the northwestern parts of Ellsworth Trough (Ellsworth Subglacial Lake and its locale) draped over a hillshade image of the same data. Black arrows indicate the positions of hanging tributary valleys identified in bed topography data. Thin black outline (reproduced as white outlines in panels b and c) is area of Ellsworth Subglacial Lake; thick black line (also shown in panel b) is location of RES survey line C9 (see Figure 4). Ice surface contours (thin black lines), at 10 m intervals are derived from the 1 km ice surface DEM of Bamber et al., [2009]. Black box is area of bed topography data in figure 5b; (B) Subglacial bed topography around Ellsworth Subglacial Lake derived from ground-based radio-echo sounding data. Contours are in 200 m intervals; (C) Profile curvature of the MODIS MOA imagery; (D) Ice surface elevation of survey line C9; (E) Ice thickness of survey line C9; (F) Bed elevation of survey line C9; (G) values of MODIS ice surface imagery extracted along survey line C9.

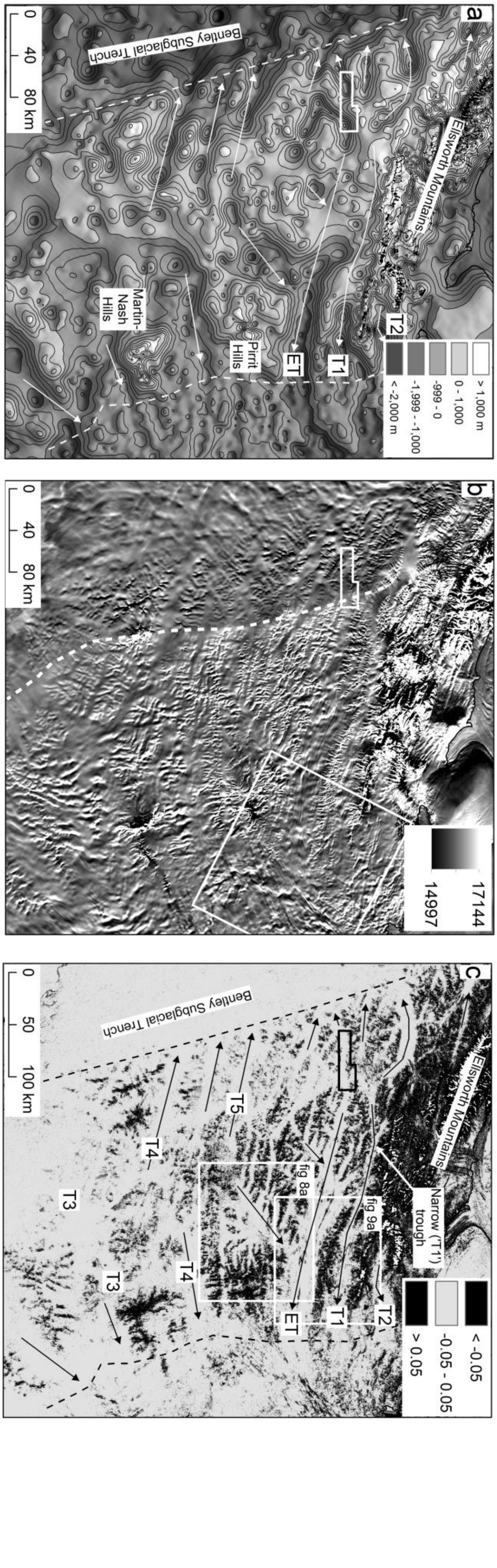
a
Bentley Subglacial Trench
Ellsworth Mountains
Martin-Nash Hills
Pirrit Hills
ET
T1
T2
> 1,000 m
0 - 1,000
-999 - 0
-1,999 - -1,000
< -2,000 m
0 40 80 km
b
0 40 80 km
17144
14997
c
Bentley Subglacial Trench
Ellsworth Mountains
Narrow ('T1') trough
fig 8a
fig 9a
T1
T2
T3
T3
T4
T4
T5
ET
< -0.05
-0.05 - 0.05
> 0.05
0 50 100 km

Figure 6: (A) Subglacial topography of the Ellsworth Subglacial Highlands (BEDMAP2) [Fretwell et al., 2013]. White arrows show the broad paleo-ice-field ice-flow regime inferred from the ice surface imagery and the subglacial topography data. Dashed white lines show the inferred ice field limit; (B) MODIS MOA ice surface imagery [Haran et al., 2006]. White dashed line shows approximate position of present-day ice divide. Small white box shows the extent of the RES survey around Ellsworth Subglacial Lake. Large white box is the area of Figure 3c; (C) Profile curvature analysis map of MODIS MOA ice surface data. Black arrows show the broad ice-field ice flow regime inferred from the ice surface imagery and the subglacial topography data. Dashed black lines show the inferred ice field limit. White boxes show extent of Figures 8a and 9a; Figures 6a, 6b and 6c have the same extent as Figures 1b and 7a.

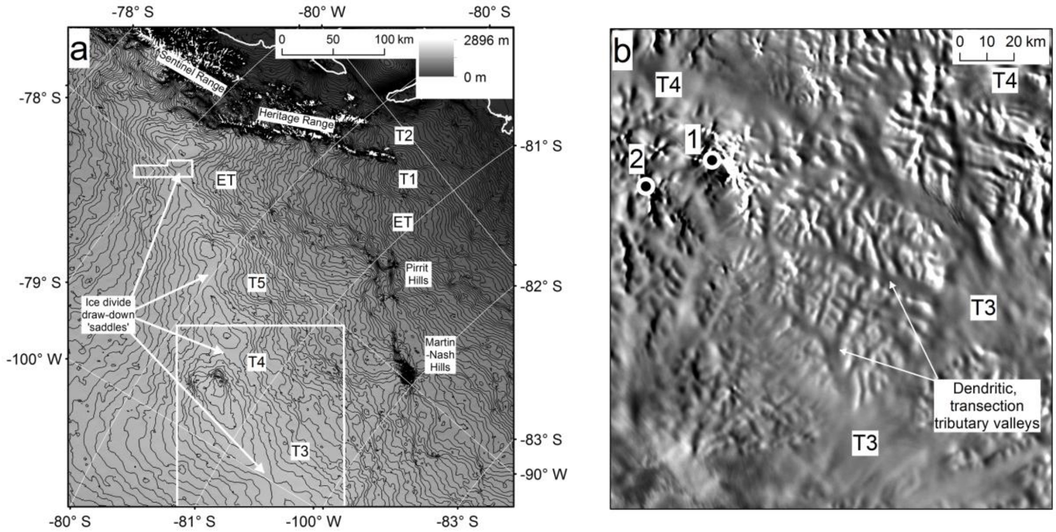

Figure 7: (A) Ice sheet surface elevation over the Ellsworth Subglacial Highlands derived from GLAS/ICESat 500 m Laser Altimetry Digital Elevation Model of Antarctica [DiMarzo et al., 2007] (extent of Figure 7a is the same as Figures 6a-c and 1b). Contours are in 20 m intervals. Large white box shows extent of 7b, small white box shows extent of ground-based RES around Ellsworth Subglacial Lake; (B) MODIS MOA surface morphology imagery [Haran et al., 2006] of the area to the south of Mount Moore (1) and Mount Woollard (2) showing dendritic network of transection valleys. Note correspondence between drawn-down parts of the ice divide in 7a and the smooth areas of the optical imagery, believed to represent deep subglacial troughs, in 7b.

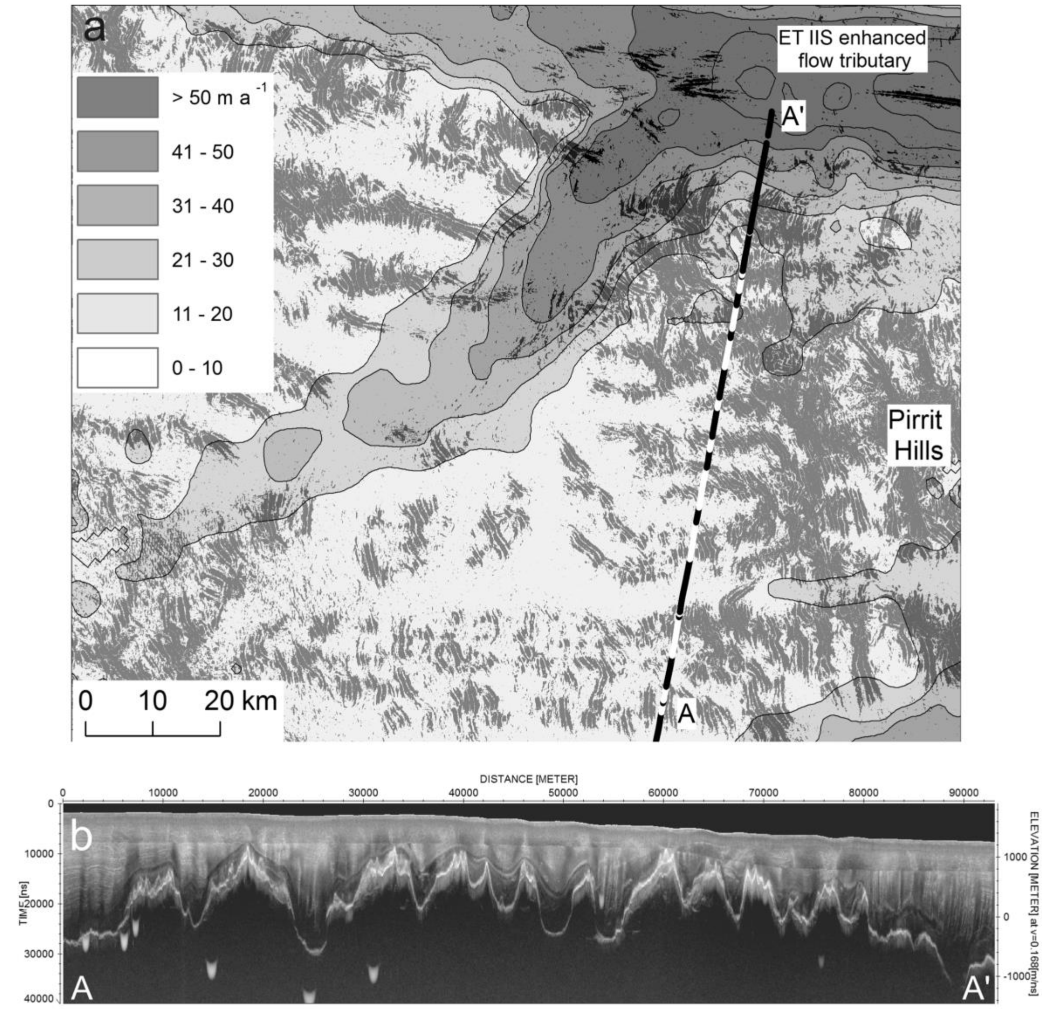

Figure 8 (A) Profile curvature analysis map of MODIS MOA ice surface data with ice sheet surface velocity map [Rignot et al., 2011] superimposed. Cells with curvature <-0.05 and >0.05 are colored black, cells with curvature between -0.05 and 0.05 are colored light grey. Line A-A' shows survey line of radargram in 8b. Black sections of line show topography <250 m asl (i.e. deep valleys), white sections topography >250 m asl (i.e. subglacial highlands). The profile curvature map clearly reflects the subglacial topography beneath; (B) Radargram (A-A’) showing subglacial topography of the northern side of the Pirrit Hills. The ice flow that cut these U-shaped valleys is inferred to have been into the radargram, from the Pirrit Hills towards the broad basin that feeds the Ellsworth Trough (ET).

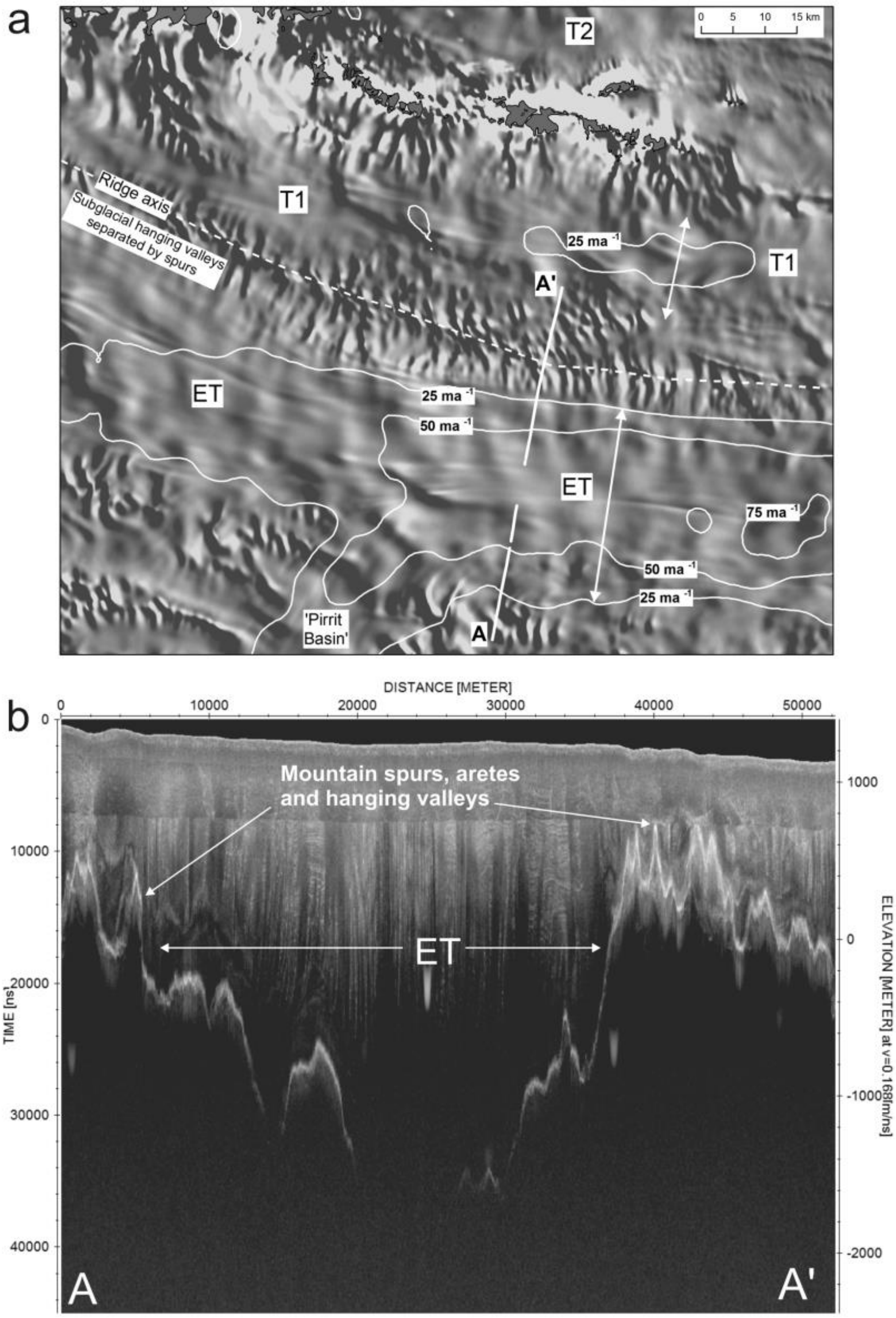

Figure 9: (A) MODIS MOA ice surface imagery of a ~100 km long subglacial mountain ridge which separates the Ellsworth Trough (ET) from the adjacent valley T1 (‘Narrow’ trough). The mountain ridge is adorned with a series of subglacial hanging valleys, separated by arêtes, which are tributaries of these troughs. The Ellsworth Trough (ET) hosts an enhanced flow tributary of the Institute Ice Stream. Contours

(at 25 m intervals) of present-day ice surface velocities (Rignot et al., 2011), are superimposed to demonstrate the importance of these geomorphic features in controlling present-day ice flow. Grey filled polygons represent areas of exposed bedrock (from Antarctic Digital Database (ADD)). Broad white line (A-A') across trough and adjacent ridges marks the location of radargram in 9b. Present-day ice flow along the troughs (ET, T1 and T2) is approximately left to right; (B) Radargram showing the deep Ellsworth Trough (ET) bounded by mountainous subglacial topography with hanging valleys, arêtes and mountain spurs. Present-day ice flow is approximately out of page. Note that the bed is not sounded in the deepest parts of the trough, which in this radargram represents bed below ~1600 m below sea level (section without data is represented by the break in line A-A’ in 9a).